NMR and NIR Studies of the Tautomerism of 5,10,15,20-Tetraphenylporphyrin including Kinetic HH/HD/DD Isotope and Solid State Effects

Martin Schlabach[1], Bernd Wehrle[2], Helmut Rumpel[3], Jürgen Braun[4], Gerd Scherer[4], and Hans-Heinrich Limbach[4*]

Institut für Physikalische Chemie der Universität Freiburg, Albertstraße 21, W-7800 Freiburg, Germany

Chemical Kinetics / Isotope Effects / Proton Transfer / Solid State Effects / Spectroscopy, Nuclear Magnetic Resonance

The liquid and solid state tautomerism of 5,10,15,20-tetraphenylporphyrin-$^{15}N_4$ (meso-tetraphenylporphyrin, TPP) has been studied by dynamic NMR spectroscopy and by NIR spectroscopy. The kinetic HH/HD/DD isotope effects on the liquid state tautomerism were reinvestigated in the temperature region between 200 K and 300 K. It was confirmed that the kinetic HH/HD isotope effects are large and the HD/DD isotope effects small. At 298 K the values 9.7 and 1.8 were obtained. The Arrhenius curve of the HH reaction is non-linear indicating that the proton transfer takes place by thermally activated tunneling at low temperatures. The kinetic isotope effects are consistent with a stepwise proton transfer pathway involving intermediate tautomeric states in which protons are bound to adjacent nitrogen atoms. Solid state NMR experiments were performed on triclinic TPP, where the reaction barrier is higher compared to TPP in the liquid state. In addition, the degeneracy of the tautomerism in the solid state is lost due to intermolecular interactions. The latter conclusion is supported by the finding that for tetragonal mixed crystals of $[(TPP-{}^{14}N_4-Ni)_{0.1}(TPP-{}^{15}N_4-H_2)_{0.9}]$ the degeneracy of the tautomerism and its barrier is equal to the values found for the liquid solution. The NIR measurements show the presence of NH-stretching overtones in the region of about 6450 cm^{-1}. The anharmonicity of this vibration is of the usual order, which indicates that the reaction coordinate of proton transfer is not identical with the normal modes of the NH-stretching vibrations, but rather a combination of various vibrational modes including the stretching, bending and skeletal modes. As a consequence, there will be a large number of vibrational states from which tunneling might occur.

1. Introduction

The problem of proton tautomerism of porphyrins in the liquid and solid state (Fig. 1) has received considerable attention. The process was first monitored in 1973 by Storm et al. using ^1H NMR spectroscopy of 5,10,15,20-tetraphenylporphyrin (meso-tetraphenylporphin, TPP) dissolved in organic solvents [1–3]. Rate constants of the thermal reaction of porphyrins dissolved in organic solvents have been obtained by NMR lineshape analysis [4–7], relaxation time measurements [7, 8] and magnetization transfer experiments in the laboratory [9] and the rotating frame [10]. The reaction was shown to exhibit strong kinetic HH/DD isotope effects [4, 7]. In 1982 NMR-methods for the determination of full kinetic HH/HD/DD isotope effects on degenerate double proton transfer reactions were designed in this laboratory [11]. Unfortunately, these methods were not yet as precice as desirable at that time because of the use of a low field NMR-spectrometer. Nevertheless, it was already found that the kinetic HH/HD isotope effect is very large, i.e. of the order of 10 and the HD/DD isotope effect very small, i.e. of the order of 1 [11]. These results were initially interpreted in terms of a concerted double proton transfer pathway involving proton tunneling [12–14]. Subsequent theoretical studies [15–18] and also one experimental study [19, 20] gave, however, evidence, that the two protons are transfered stepwise involving the cis tautomers as shown in Fig. 2. Recently, progress has been made in the understanding of kinetic isotope effects of symmetric double proton transfer reactions [21–27] which predict for the case of the tautomerism of porphyrins at least a small kinetic HH/HD isotope effect of the order of 2. One scope of this study is, therefore, to reinvestigate the full kinetic HH/HD/DD isotope effects of the tautomerism of TPP with a higher precision in order to decide whether the theoretically proposed reaction pathway can be supported experimentally.

The second problem which will be addressed in this study concerns the problem of how the tautomerism of TPP is affected by intermolecular interactions in the solid state. The solid state tautomerism of porphyrins was discussed some

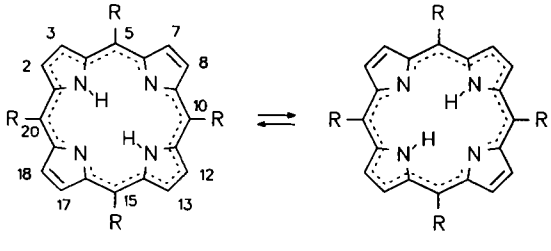

Fig. 1
The tautomerism of 5,10,15,20-tetraphenylporphyrin (meso-tetraphenylporphyrin, TPP)

[1] Present address: Norwegian Institut for Air Research, N-2001 Lillestrøm, Norway.
[2] Present address: Fa. Bayer AG, D-5900 Leverkusen.
[3] Present address: Kinderspital Zürich, Steinwiesstraße 75, CH-8032 Zürich, Switzerland.
[4] Present address: Fachbereich Chemie, Freie Universität Berlin, Takustraße 3, W-1000 Berlin 33, Germany.
*) Author for correspondence.

  0005-9021/92/0606-0821 $ 3.50+.25/0

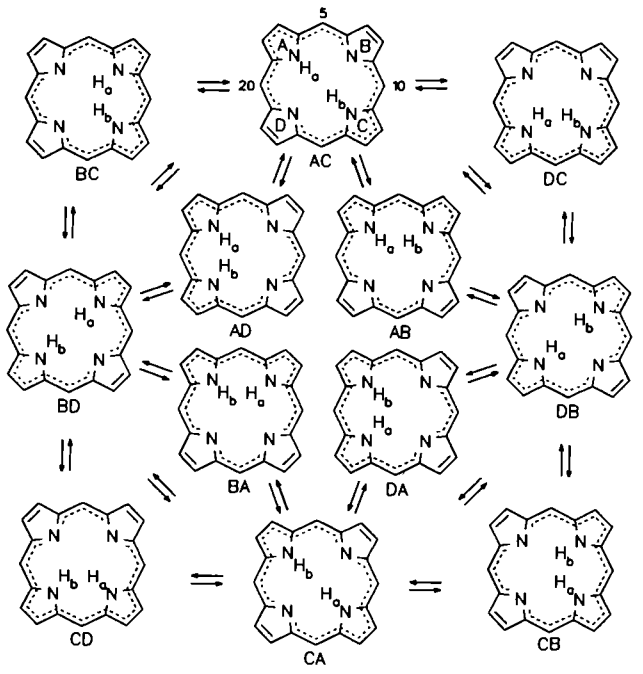

Fig. 2
Proton Transfer pathways in porphyrins according to Ref. [21]. The different tautomers are labeled according to the pyrrole rings to which the mobile protons are attached. Observable species are the degenerate trans-tautomers AC, BD, DB, and CA

time ago in crystallographic studies on this class of compounds [28–33]. Optical studies of porphyrins embedded in Shpolski matrices [20, 34–36] revealed that free-base porphyrins are indeed subject to a phototautomerism in the solid state. Using high resolution solid state ^{15}N NMR spectroscopy under the conditions of cross polarization (CP) and magic angle spinning (MAS) [37–39] it was shown in 1984, that porphyrins are also subject to a thermal tautomerism in the crystalline state and rate constants were reported for these systems [40]. Rate constants were also reported for the parent compound porphyrin [41] and related systems [42–51]. Low temperature thermal rate constants of porphyrin were obtained recently also using optical methods [19, 20].

The main result of the solid state ^{15}N CPMAS NMR studies is that, in principle, the degeneracy of the process shown in Fig. 1 is lost in the solid state, e.g. in the case of triclinic TPP [40] or other substituted porphyrins [49, 50]. By contrast, symmetric or quasi-symmetric situations were found for 5,10,15,20-tetratolylporphyrin [40] and for the parent compound porphyrin [41, 49]. These solid state perturbations have not yet been studied in detail. This knowledge is necessary in the constructing of a single Arrhenius curve for the same process based on kinetic data obtained from different liquid and solid environments [19, 20]. Also, they could give information about the question as to whether the loss of degeneracy of the proton transfer in solid porphyrins is an intrinsic molecular property or whether they arise from intermolecular interactions. The first case could be realized if the proton transfer in Fig. 1 was accompanied by a conformational change of the molecular skeleton suppressed in the solid state. In other words, the question arises, whether it is possible to influence the reaction energy surface of the tautomerism of porphyrins such as TPP by placing the reactive molecule in a solid environment with a higher symmetry.

A clue to answering this question may be obtained through the observation by X-ray crystallography, that metal (Me^{2+}) containing porphyrins can adopt a tetragonal crystal symmetry. An especially interesting case is the mixed crystal system $[(TPP\text{-}Ag)_x(TPP\text{-}H_2)_{1-x}]$ which can be regarded as a solution of TPP-Ag in TPP or vice versa [52, 53]. Whereas the pure compounds with $x = 0$ and 1 form triclinic crystals, the solid solutions cannot only crystallize in a triclinic, but to a minor extent ($\sim 1\%$) also in a stable tetragonal form in the range $0.08 < x < 0.54$. The molecular symmetry of the tetragonal form is of the S_4 type, so one could expect the two tautomeric forms of free base TPP to be equally populated in the solid solution. We therefore presumed that the study of the tautomerism of free base TPP in tetragonal $[(TPP\text{-}Me)_x(TPP\text{-}H_2)_{1-x}]$ solutions by solid state NMR spectroscopy, should lead to interesting insights into the question of how easily the solid state tautomerism of this class of molecules can be manipulated by a change of the environment. Unfortunately, however, TPP-Ag is not the best model system for such studies for two reasons. Firstly, Ag^{2+} is paramagnetic, which may lead to undesired paramagnetic shifts and line broadening. On the other hand, the small yield of 1% per crystallization process is unsatisfactory. We therefore decided to prepare and characterize tetragonal $[TPP\text{-}Ni)_x(TPP\text{-}H_2)_{1-x}]$, which has not yet been described. This material is formed in a higher yield as compared to the corresponding silver derivative. In order to avoid undesired ^{15}N lines from TPP-Ni, we allowed non-labeled TPP-Ni-$^{14}N_4$ to co-crystallize with labeled TPP-H_2-$^{15}N_4$. ^{15}N CPMAS NMR experiments were then performed on the resulting $[(TPP\text{-}Ni\text{-}^{14}N_4)_x\text{-}TPP\text{-}H_2\text{-}^{15}N_4)_{1-x}]$ as a function of temperature. We found that the degeneracy of the tautomerism is restored in this material within the margin of error of the NMR method, thus allowing us to directly compare the liquid and solid state rate constants of TPP. For comparison, we also studied triclinic TPP. Only preliminary rate constants have previously been reported for this compound [40]. Triclinic TPP serves as a model as to how solid state perturbation influences the reaction coordinate.

The last problem to be treated in this publication relates to the number and nature of the relevant vibrational states on both sides of the barrier of proton transfer. For this purpose, near infrared (NIR) experiments were performed on TPP in the solid state.

The next section deals firstly with the description of the synthesis of the labeled compounds studied, as well as the experimental details of the NMR and NIR experiments. A report is then given on the results of the kinetic measurements on TPP in the liquid state, including the HH/HD/DD isotope effects and the results of the solid state experiments. Finally, the results are discussed.

2. Experimental

2.1 Synthesis of ^{15}N-labeled Compounds

2.1.1. 5,10,15,20-Tetraarylporphyrin-$^{15}N_4$

The ^{15}N labeled tetraarylporphyrins were synthesized by modifying the recipes for the unlabeled compounds [54, 55] from pyrrole-^{15}N enriched to 95% and purchased from A. H. Hempel GmbH, Düsseldorf. As an example we describe the synthesis of TPP-$^{15}N_4$.

To 16 ml of boiling propionic acid, 0.5 ml of freshly recondensed pyrrol-^{15}N and 0.74 ml of freshly destilled benzaldehyde were added. After refluxing of the reaction mixture for 30 min and cooling to room temperature, the precipitate was filtered and washed several times with methanol. The product was air dried and recrystallized in an exsiccator by slowly evaporating the solvent. Finally, the crystals were dried in vacuo. We obtained a yield of 188 mg, i.e. 16.9% of the theoretical yield.

During the synthesis of the tetraarylporphyrins, the corresponding tetraarylchlorins are by-products of the reaction. The amount of chlorin can be determined by UV spectroscopy. The lowest energy absorption Q-band of chlorin-free TPP appears at 647 nm, whereas a shoulder at 650 nm appears in chlorin containing TPP [56]. The chlorin impurity can be oxidized to the porphyrin with 2,3-dichloro-5,6-dicyanobenzoquinone (DDQ) [56]. We used the following procedure: 180 mg of chlorin containing TPP are dissolved in 45 ml of boiling CH_2Cl_2. A solution of 48 mg DDQ in 2.7 ml benzene is then added and the mixture refluxed for 30 min. After evaporation of the solvent, the greenish/violet residue is purified by chromatography over neutral alumina with chloroform as a solvent. The different TPP fractions are unified and concentrated. TPP is then precipitated by adding 20 ml methanol. The dried product no longer contained the chlorin band in the UV/Vis spectrum.

2.1.2. Synthesis of the Tetragonal Mixed Crystal System [(TPP-Ni-$^{14}N_4$)$_{0.1}$(TPP-H_2-$^{15}N_4$)$_{0.9}$]

Ni-TPP was prepared from TTP and $NiCl_2 \times 6H_2O$ in dimethylformamide according to Ref. [57]. The reaction was followed by thin-layer chromatography. The Ni complex was purified by chromatography over neutral alumina (activity III) using chloroform as a solvent. The compound was slowly recrystallized from dichloromethane and was characterized by its UV-spectrum (λ_{max} = 525 nm), as well as by mass spectroscopy (M = 670‡).

Tetragonal mixed crystals of the system [(TPP-Ni-$^{14}N_4$)$_x$(TPP-H_2-$^{15}N_4$)$_{1-x}$] were prepared by dissolving the purified components (e.g. 20 mg ^{15}N-TPP and 3 mg Ni-TPP) in chloroform and by slow evaporation of the solvent. During this process, not only did tetragonal crystals appear, but also some octahedral crystals. The latter were removed with the help of a pair of tweezers and a magnifying glass.

The purity and composition of the mixed crystals were determined by mass spectroscopy. It was found that the crystals contained ^{14}Ni-TPP to about 10%, i.e. that they corresponded to the structure [(TPP-Ni-$^{14}N_4$)$_{0.1}$(TPP-H_2-$^{15}N_4$)$_{0.9}$]. The ^{15}N CPMAS NMR spectra later showed that the crystals did not contain any Ni-TPP-$^{15}N_4$ in observable amounts.

Since in the literature no mixed crystal system of the components between TPP-Ni and free base TPP were described, the crystal symmetry of the mixed crystals was determined. For this purpose the Laue diagrams were measured for different crystal orientations. These diagrams are projections of the crystal planes (hkl) and reflect directly the symmetry of the crystal. The Laue group was determined to be 4/mmm. From the conditions for observable reflexes, $h + k + l = 2n$, $2h + 1 = 4n$ and $h \neq 2n$ only the space groups $I4_1md$ and $I\bar{4}2d$ were possible. The dimensions of the elementary unit a = 15.11, c = 13.98 Å, were determined by powder diffractometry ($Mo_{K\alpha}$, λ = 0.703 Å), by least squares fit of the experimental and calculated dependence of the reflexes as a function of the diffraction angle. From the volume of the unit cell $U = 4 \times 798$ Å^3 we conclude that there are $Z = 4$ equivalent molecules in the unit cell. These results are in good agreement with the dimensions of the pure phases, Ni-TPP [58] (a = 15.04, c = 13.92 Å, $U = 4 \times 787$ Å^3) and of the tetragonal modification of TPP described by Hamor et al. [31] (a = 15.125 ± 0.125, c = 13.94 ± 0.02 Å, $U = 4 \times 797$ Å^3). Both phases belong to space group $I\bar{4}2d$ with four molecules in the unit cell, which is in good agreement with the findings of the system studied here. Therefore, the structure of [(TPP-Ni-$^{14}N_4$)$_{0.1}$(TPP-H_2-$^{15}N_4$)$_{0.9}$] is very close to the structure of tetragonal TPP which also contained some tetragonal metal-TPP [31].

2.2. NMR and NIR Measurements

The liquid state NMR experiments were performed with a Bruker NMR spectrometer MSL 300 working at 300.13 MHz for protons and at 75 MHz for ^{13}C. The ^{13}C spectra were measured using WALTZ-16-^{1}H-decoupling in order to minimize heating of the sample. The solid state NMR experiments were performed on a Bruker CXP 100 NMR spectrometer equipped with a 2.1 T wide-bore cryomagnet corresponding to a frequency of 90.02 MHz for ^{1}H and of 9.12 MHz for ^{15}N. For the CPMAS NMR experiments, a MAS probe from Doty-Scientific, Columbia, South Carolina was employed. The spinning speeds were always in the 2 to 3 kHz range. In the low temperature experiments, the driving nitrogen gas was cooled with liquid nitrogen with a home-built heat exchanger described elsewhere [42]. The sample temperature was monitored with a Pt resistance thermometer placed close to the sample.

The NIR experiments on triclinic TPP were taken in the diffuse reflection mode of a TPP/KCl powder using a Bruker Fourier transform infrared (FT-IR) spectrometer IFS 113 V, in a similar way as has been described previously [26].

3. Results

3.1. Kinetic HH/HD/DD Isotope Effects on the Tautomerism of 5,10,15,20-tetraphenylporphyrin-$^{15}N_4$(TPP) Dissolved in Organic Solvents

In this section, we re-investigate the kinetic HH/HD/DD isotope effects on the tautomerism of TPP dissolved in organic solvents, using dynamic ^{1}H and ^{13}C NMR spectroscopy. The rate constants of the tautomerism of TPP can be defined in different ways. In previous studies [4, 7–10, 19, 20, 40, 45] the symmetric rate constants k were based on the reaction shown in Fig. 1. The k values have to be related to the rate constants of the individual reaction steps of the extended reaction network shown in Fig. 2. In the latter, the different tautomers are labeled according to the pyrrole rings to which the mobile protons are attached. The rate constant of the reaction of tautomer MX to NY is then written as $k_{MX \to NY}$. Observable species are the degenerate trans-tautomers AC, BD, DB, and CA. As can easily be shown, the relation

$$k = 2k_{AC \to DB} = 2k_{AC \to BD} = 2k_{BD \to CA} = 2k_{DB \to CA} . \quad (1)$$

is valid.

3.1.1. ^{1}H and ^{13}C NMR Lineshape Analysis of TPP Dissolved in Organic Solvents at Different Deuterium Fractions

The temperature dependence of the signals of the inner hydrogen atoms of ^{15}N labeled TPP has been described previously [3, 7], including the theory of extracting the rate constants from the lineshapes [7]. In a subsequent study, ^{1}H NMR experiments were performed on these signals not only at deuterium fraction D of the inner proton sites at D = 0 [7] but also at $D > 0.9$ [11], from

which the constants $k^{HH} = 2k^{HH}_{AC\to DB}$ and $k^{HD} = 2k^{HD}_{AC\to DB}$ were obtained. Because of signal-to-noise problems associated with the high value of D and the low ^1H frequency employed the latter were not very precise. We have, therefore, re-measured both $k^{HH}_{AC\to DB}$ and $k^{HD}_{AC\to DB}$ with improved accuracy. In additional dynamic ^{13}C NMR experiments, rate constants, $k^{HH} = 2k^{HH}_{AC\to DB}$ and $k^{DD} = 2k^{DD}_{AC\to DB}$ were determined.

Figs. 3 and 4 show the superposed experimental and calculated ^1H NMR signals of the inner protons of TPP dissolved in toluene-d_8 at deuterium fractions of $D = 0$ and 0.85 in the mobile proton sites. These signals appear at $\delta \approx -2.3$ ppm. They were calculated as described previously [7]. The intramolecular proton transfer gives rise to a doublet-pentet transition when going from the slow to the fast exchange regime [4, 7]. The coupling constant $J_{^1H-^{15}N}$ and the residual line width in the absence of exchange, W_0, can be obtained by simulation of the outer line components. At $D = 0$, the line shapes depend on $2k^{HH}_{AC\to DB}$, at $D = 0.85$ mostly on $2k^{HD}_{AC\to DB}$. Naturally, the signal-to-noise ratio is not as good at $D = 0.85$ compared to $D = 0$. In calculating the spectra, the presence of residual amounts of TPP-HH was taken into account, determined by integration of the inner to the β-pyrrole proton signals positions in Fig. 1).

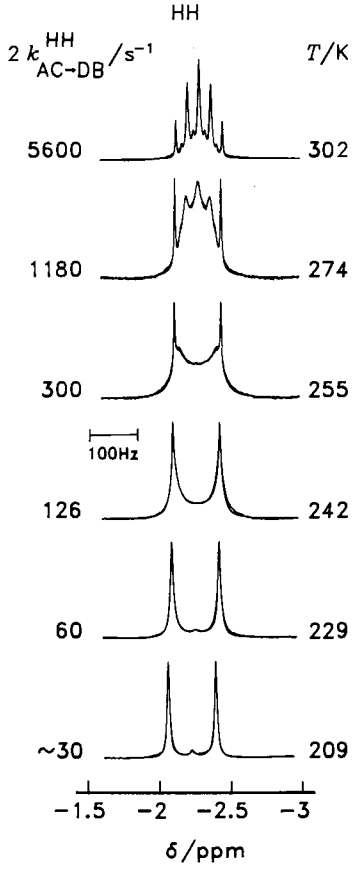

Fig. 3
Superposed experimental and calculated 300.13 MHz ^1H NMR spectra of the inner protons of 5,10,15,20-tetraphenylporphyrin-$^{15}N_4$ dissolved in toluene-d_8 (~10 mMol/l), at a deuterium fraction $D = 0$ of the inner proton sites. 3 μs π/2-pulses, 6 kHz spectral width, 3.5 s repetition time, up to 7000 scans

Figs. 5 and 6 contain the results of the ^{13}C NMR lineshape analysis performed on the β-pyrrole carbon signals of TPP dissolved in tetrahydrofuran. These signals appear at $\delta \approx 131$ ppm und $\delta \approx 137$ ppm. The o-, m-, and p-phenyl carbon signals are not affected by the exchange. At $D = 0.9$ and 259 K, the deuteron transfer is so slow that the splitting of the two non-equivalent β-pyrrole carbons can easily be observed. In the intermediate temperature range, i.e. the coalescence region, it is extremely difficult to detect the very broad signal hidden by the noise. The kinetic HH/DD isotope effect is clearly demonstrated in the two sets of spectra in Figs. 5 and 6.

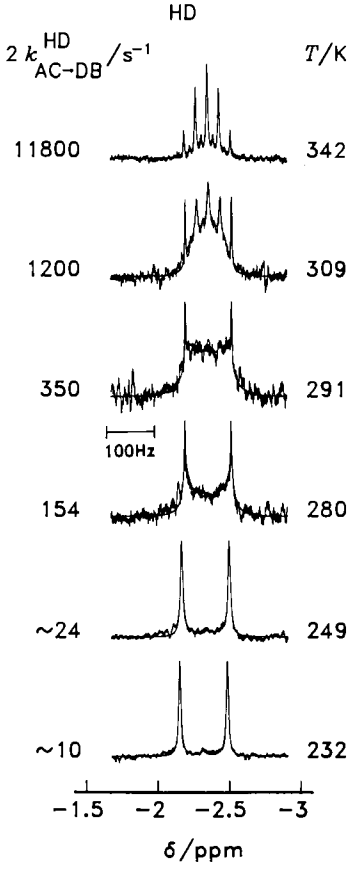

Fig. 4
Same as 3, but at a deuterium fraction $D = 0.85$ of the inner proton sites

The data obtained here are assembled in Table 1 which also contains published values of $2k^{HH}_{AC\to DB}$ which we estimate to exhibit only small systematic errors. These are rate constants obtained by lineshape analysis of the inner proton signal in a similar way as shown in Fig. 3 [7], obtained by lineshape analysis of the β-pyrrole signals in the coalescence regime [7], derived from the β-pyrrole proton $T_{1\varrho}$ values in the frequency dispersion region [7] and determined by magnetization transfer of the latter signals in the rotating frame [10]. These selected older data are in good agreement with the data obtained here using improved methods. The published rate constants of the HD- and DD-transfer processes obtained at 2.1 T were neglected, because their precision was much poorer due to signal noise problems and the limited chemical shift range as compared with this study. From the data in Table 1 we constructed Arrhenius curves of the HH, the HD and the DD migration. By linear least squares fitting of the data we obtained:

$$k^{HH} = 2k^{HH}_{AC\to DB} = 10^{10.7\pm0.2}\exp(-39.6\pm0.7\ \text{kJ mol}^{-1}/RT), \quad (2)$$
$$198\ \text{K} \le 340\ \text{K},\ 2k^{HH}_{AC\to DB}(298) \approx 5600\ \text{s}^{-1},$$

$$k^{HD} = 2k^{HD}_{AC\to DB} = 10^{12.1\pm0.3}\exp(-53.1\pm1.4\ \text{kJ mol}^{-1}/RT), \quad (3)$$
$$259\ \text{K} \le T \le 342\ \text{K},\ 2k^{HD}_{AC\to DB}(298) \approx 580\ \text{s}^{-1},$$

$$k^{DD} = 2k^{DD}_{AC\to DB} = 10^{12.2\pm0.5}\exp(-55.1\pm2.7\ \text{kJ mol}^{-1}/RT), \quad (4)$$
$$259\ \text{K} \le T \le 342\ \text{K},\ 2k^{DD}_{AC\to DB}(298) \approx 330\ \text{s}^{-1}.$$

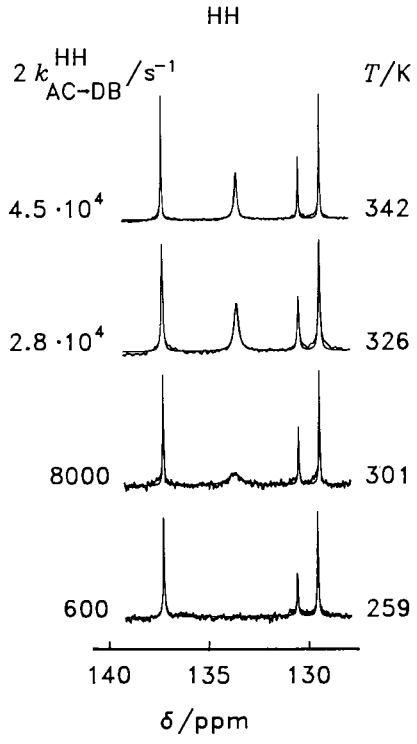

Fig. 5
Superposed experimental and calculated 75 MHz ^{13}C NMR spectra of the β-pyrrole ^{13}C atoms of TPP dissolved in tetrahydrofuran-d_8 at a deuterium fraction of $D = 0$ in the inner proton sites. 4 μs π/2-pulses, 13 kHz spectral width, 3.6 s repetition time, ^{1}H-WALTZ-decoupling, up to 40000 scans

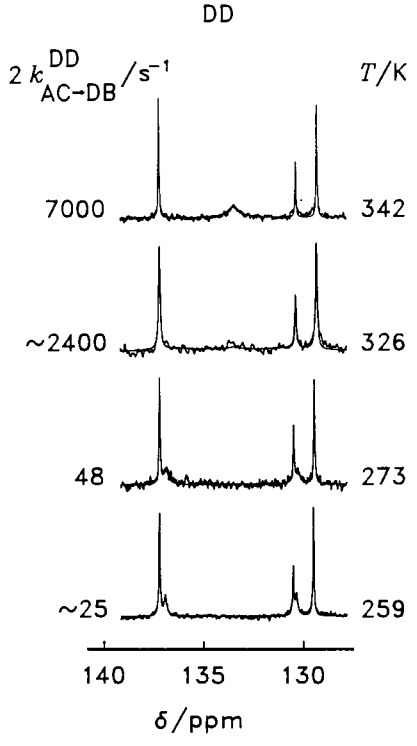

Fig. 6
Same as Fig. 5 but at a deuterium fraction of $D = 0.9$ in the inner proton sites

From these equations we obtained the following kinetic isotope effects

$$k^{HH}/k^{HD} \approx 9.7\,,\ k^{HH}/k^{DD} \approx 17.2\,,\ k^{HD}/k^{DD} \approx 1.8\,. \tag{5}$$

at 298 K.

As discussed below, the Arrhenius curve of the HH process is not well represented by the linear Eq. (2), but shows a marked curvature. It was ensured that this non-linear behavior was genuine and did not arise from slow molecular tumbling which shortens the transverse relaxation times [8–10].

3.2. Solid State ^{15}N CPMAS NMR Studies of ^{15}N Labeled 5,10,15,20-tetraphenyl-porphyrin-$^{15}N_4$ in Different Phases

In this section we report the results of the solid state ^{15}N NMR studies on (i) triclinic 5,10,15,20-tetraphenylporphyrin (TPP) and TPP embedded in TPP-Ni.

3.2.2. Triclinic TPP

In Fig. 7 the 9.12 MHz ^{15}N CPMAS NMR spectra of triclinic TPP are shown as a function of temperature. Two sharp singlets characterized by the chemical shift difference $\Delta\nu$ are observed at low temperature. As the temperature is raised, the lines broaden and sharpen again without coalescence and move towards each other showing a reduced line splitting $\delta\nu$. Obviously, the degeneracy of the tautomerism is lost, as in the case of triclinic TPP, where the observation of two averaged ^{15}N lines at different frequencies indicates two types of nitrogen atoms with differing average proton densities, due to the fact that the equilibrium constant $K_{12} \equiv K_{AC\rightarrow DB}$ of the tautomerism is no longer equal to 1. It has previously been shown [40, 44, 47, 51] that

$$K_{12} = (1-\delta\nu/\Delta\nu)/(1+\delta\nu/\Delta\nu)\,. \tag{6}$$

$\delta\nu$ was measured at different temperatures and the equilibrium constants were calculated according to Eq. (6). The results and previously obtained data [40] are in good agreement and are listed in Tables 2 and 3. The temperature dependence of the rate constants was found to be given by

$$\begin{aligned} \ln K_{12} \equiv \ln K_{AC\rightarrow DB} &= 1.013 - 905.4/T\,, \\ K_{12} \equiv K_{AC\rightarrow DB}(298\,\mathrm{K}) &= 0.132\,, \end{aligned} \tag{7}$$

from which a reaction enthalpy $\Delta H_{AC\rightarrow DB} = 7.5 \pm 1.2$ kJ/mol and a reaction entropy of $\Delta S_{AC\rightarrow DB} = 8.8 \pm 3.8$ J/Kmol was calculated.

Eq. (7) provided the populations necessary to calculate the exchange broadened spectra at low temperatures, using a lineshape theory described recently in detail [51]. The resulting rate constants are listed in Table 3. We obtained

$$\begin{aligned} k_{12} \equiv k^{HH}_{12} &= 2k^{HH}_{AC\rightarrow DB} \\ &= 10^{12.2\pm0.4}\exp(-52.9 \pm 1.9\ \mathrm{kJ\,mol^{-1}}/RT)\,, \\ &262 \le T \le 310\,\mathrm{K}\,,\ 2k^{HH}_{AC\rightarrow DR}(298\,\mathrm{K}) = 850\,\mathrm{s^{-1}}\,. \end{aligned} \tag{8}$$

The rate constants of the backward reaction are then given by a combination of Eqs. (7) and (8):

$$\begin{aligned} k_{21} = k^{HH}_{21} &= 2k^{HH}_{DB\rightarrow AC} \\ &= 10^{12.1\pm0.5}\exp(-47.3 \pm 2.8\ \mathrm{kJ\,mol^{-1}}/RT)\,, \\ &262 \le T \le 310\,\mathrm{K}\,,\ 2k^{HH}_{DB\rightarrow AC}(298\,\mathrm{K}) = 6440\,\mathrm{s^{-1}}\,. \end{aligned} \tag{9}$$

Table 1
Results of the dynamic ^{1}H- und ^{13}C-NMR-experiments performed on TPP in liquid solution

T/K W_0/Hz	Solvent	Method	k^{HH}/s^{-1}	k^{HD}/s^{-1}	k^{DD}/s^{-1}	D	$\Delta\nu$/Hz	W_0/Hz
198	THF	MTRF	2.3	–	–	0	–	
203	THF	MTRF	2.9	–	–	0	–	
229	Tol	NH	60	–	–	0	99.9	3.3
242	Tol	NH	126	–	–	0	98.2	3.3
249	Tol	NH	196	–	–	0	98.1	3.4
255	Tol	NH	304	–	–	0	97.5	3.2
274	Tol	NH	1180	–	–	0	96.5	3.2
302	Tol	NH	5600	–	–	0	97.2	3.1
273	THF	NH	1400	–	–	0	101.0	–
293	THF	NH	7000	–	–	0	101.0	–
250	THF	$T_{1\varrho}$	243	–	–	0	–	–
270	THF	$T_{1\varrho}$	1120	–	–	0	–	–
280	THF	$T_{1\varrho}$	1740	–	–	0	–	–
259	THF	NH	440[1]	28	–	0.6	98.6	3.7
273	THF	NH	1060[1]	78	–	0.6	97.9	3.5
285	THF	NH	2200[1]	200	–	0.6	97.0	3.0
301	THF	NH	5800[1]	500	–	0.6	97.0	3.5
272	Tol	NH	1040[1]	77	–	0.85	97.4	3.0
280	Tol	NH	1800[1]	154	–	0.85	97.9	2.5
285	Tol	NH	2400[1]	200	–	0.85	97.1	2.5
291	Tol	NH	3800[1]	350	–	0.85	97.0	3.5
300	Tol	NH	5800[1]	700	–	0.85	96.8	3.7
309	Tol	NH	10000[1]	1200	–	0.85	96.8	2.9
321	Tol	NH	25000[1]	2400	–	0.85	96.8	2.5
331	Tol	NH	40000[1]	5600	–	0.85	96.9	2.8
342	Tol	NH	65000[1]	11800	–	0.85	96.9	2.8
72	THF	Py	1060[1]	78[2]	45	0.6/0.9	74[3]	2.0
285	THF	Py	2200[1]	200[2]	120	0.6/0.9	72[3]	2.0
301	THF	Py	5800[1]	500[2]	320	0.6/0.9	71[3]	1.9
312	THF	Py	8000[1]	860[2]	720	0.6/0.9	69[3]	1.6
259	THF	^{13}C	600[1]	–	25	0/0.9	95[3]	5.2
273	THF	^{13}C	1100[1]	160[2]	48	0/0.9	95[3]	4.9
301	THF	^{13}C	8500[1]	–	–	0/0.9	95[3]	4.6
326	THF	^{13}C	28000[1]	5500[2]	–	0/0.9	95[3]	7.6
342	THF	^{13}C	45000[1]	11800[2]	7000	0/0.9	95[3]	4.0

Solvent: Tol = toluene-d_8, THF ≙ tetrahydrofuran-d_8; Method: MTRF ≙ magnetization transfer in the rotating frame [10,11]; $T_{1\varrho}$: longitudinal relaxation time in the rotating frame [10]; NH: ^{1}H NMR line shape analysis of the ^{1}H-^{15}N signals ($\Delta\nu \triangleq {}^1J_{(H\text{-}15N)}$); Py: ^{1}H NMR line shape analysis of the β-pyrrol signals ($\Delta\nu$ ≙ difference of chemical shifts); ^{13}C: ^{13}C NMR line shape analysis of the β-pyrrole carbon atoms ($\Delta\nu$ ≙ difference of chemical shifts); $k^{LL} = 2 \cdot k^{LL}_{AC\to DB}$, LL = HH, HD und DD; D: deuterium fraction determined by ^{1}H NMR lineshape analysis; W_0: linewidth in the absence of exchange, determined by comparison of signals which do not show exchange broadening; 1: extrapolated values calculated according to Eq.(2); 2: extrapolated values calculated according to Eq.(3); 3: determined by ^{13}C-NMR lineshape analysis using k^{HH} values calculated from Eq.(2).

Table 2
Equilibrium constants K_{12} of the tautomerism in triclinic TPP

T/K	δν/ppm	K_{12}
361	68.6	0.227
343	72.4	0.197
329	75.4	0.176
310	80.7	0.149
202	108.2*)	

*) Difference of the intrinsic chemical shifts $\Delta\nu$.

3.2.3. Mixed Tetragonal Crystal System [(TPP-Ni-$^{14}N_4)_{0.1}$(TPP-H_2-$^{15}N_4)_{0.9}$]

Fig. 8 shows some representative ^{15}N CPMAS NMR spectra of tetragonal [(TPP-Ni-$^{14}N_4)_{0.1}$(TPP-H_2-$^{15}N_4)_{0.9}$] (tetragonal TPP) as a function of temperature. These spectra show a spectacular change as compared to those of triclinic TPP. We observed at high temperatures only one sharp singlet, indicating that the equilibrium constant of the tautomerism is equal to 1 within the margin of error. The analysis of the spectra is straightforward and was carried out as in the case of triclinic TTP. The kinetic data are assembled in Table 4. The following temperature dependence of the rate constants was obtained:

$$k_{12} \equiv k^{HH} = 2k^{HH}_{AC\to DB} = 10^{11.8\pm0.3}\exp(-45.4 \pm 1.4\,\mathrm{kJ\,mol^{-1}}/RT), \quad 243 \le T \le 299\,\mathrm{K},\ 2k^{HH}_{AC\to DB} = 6947\,s^{-1}. \tag{10}$$

Table 3
Rate constants k_{12} of the tautomerism of triclinic TPP

T/K	262	268	271	273	287	295	300	302	310
k_{12}/s^{-1}	55	70	120	162*)	470*)	789*)	1020	1550*)	2250

further simulation parameters: $\Delta\nu$ = 108.2 ppm; W_o = 41 Hz

*) Data from Ref. [10].

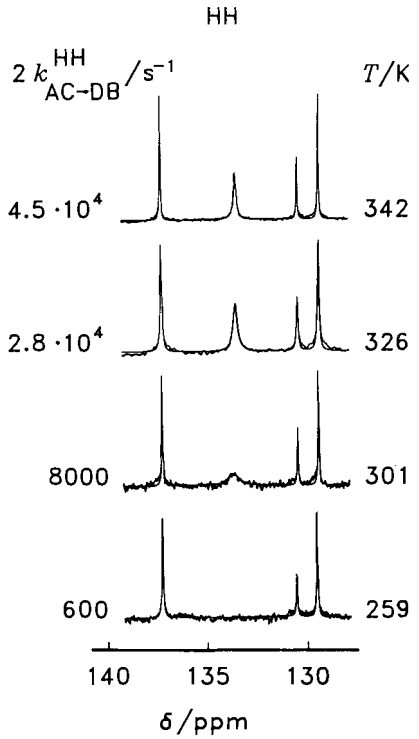

Fig. 5
Superposed experimental and calculated 75 MHz ^{13}C NMR spectra of the β-pyrrole ^{13}C atoms of TPP dissolved in tetrahydrofuran-d_8 at a deuterium fraction of $D = 0$ in the inner proton sites. 4 μs π/2-pulses, 13 kHz spectral width, 3.6 s repetition time, ^1H-WALTZ-decoupling, up to 40000 scans

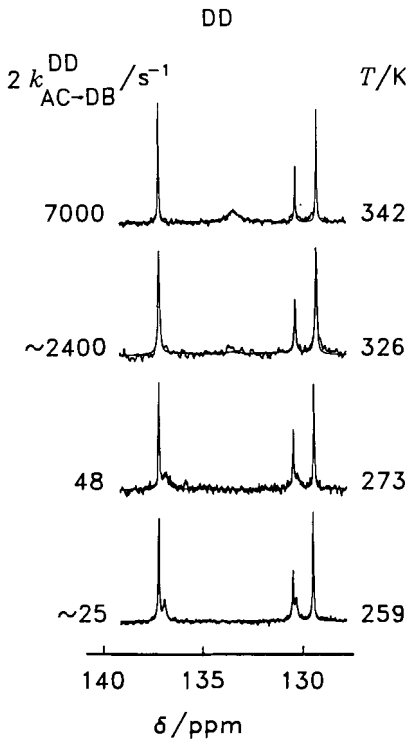

Fig. 6
Same as Fig. 5 but at a deuterium fraction of $D = 0.9$ in the inner proton sites

From these equations we obtained the following kinetic isotope effects

$$k^{HH}/k^{HD} \approx 9.7\,,\quad k^{HH}/k^{DD} \approx 17.2\,,\quad k^{HD}/k^{DD} \approx 1.8\,. \tag{5}$$

at 298 K.

As discussed below, the Arrhenius curve of the HH process is not well represented by the linear Eq. (2), but shows a marked curvature. It was ensured that this non-linear behavior was genuine and did not arise from slow molecular tumbling which shortens the transverse relaxation times [8 – 10].

3.2. Solid State ^{15}N CPMAS NMR Studies of ^{15}N Labeled 5,10,15,20-tetraphenyl-porphyrin-$^{15}N_4$ in Different Phases

In this section we report the results of the solid state ^{15}N NMR studies on (i) triclinic 5,10,15,20-tetraphenylporphyrin (TPP) and TPP embedded in TPP-Ni.

3.2.2. Triclinic TPP

In Fig. 7 the 9.12 MHz ^{15}N CPMAS NMR spectra of triclinic TPP are shown as a function of temperature. Two sharp singlets characterized by the chemical shift difference $\Delta\nu$ are observed at low temperature. As the temperature is raised, the lines broaden and sharpen again without coalescence and move towards each other showing a reduced line splitting $\delta\nu$. Obviously, the degeneracy of the tautomerism is lost, as in the case of triclinic TPP, where the observation of two averaged ^{15}N lines at different frequencies indicates two types of nitrogen atoms with differing average proton densities, due to the fact that the equilibrium constant $K_{12} \equiv K_{AC\rightarrow DB}$ of the tautomerism is no longer equal to 1. It has previously been shown [40, 44, 47, 51] that

$$K_{12} = (1-\delta\nu/\Delta\nu)/(1+\delta\nu/\Delta\nu)\,. \tag{6}$$

$\delta\nu$ was measured at different temperatures and the equilibrium constants were calculated according to Eq. (6). The results and previously obtained data [40] are in good agreement and are listed in Tables 2 and 3. The temperature dependence of the rate constants was found to be given by

$$\ln K_{12} \equiv \ln K_{AC\rightarrow DB} = 1.013 - 905.4/T\,,\qquad K_{12} \equiv K_{AC\rightarrow DB}(298\,K) = 0.132\,, \tag{7}$$

from which a reaction enthalpy $\Delta H_{AC\rightarrow DB} = 7.5 \pm 1.2$ kJ/mol and a reaction entropy of $\Delta S_{AC\rightarrow DB} = 8.8 \pm 3.8$ J/Kmol was calculated.

Eq. (7) provided the populations necessary to calculate the exchange broadened spectra at low temperatures, using a lineshape theory described recently in detail [51]. The resulting rate constants are listed in Table 3. We obtained

$$k_{12} \equiv k^{HH}_{12} = 2\,k^{HH}_{AC\rightarrow DB} = 10^{12.2\pm0.4}\exp(-52.9 \pm 1.9\ \mathrm{kJ\,mol^{-1}}/RT)\,,\quad 262 \le T \le 310\,K\,,\ 2\,k^{HH}_{AC\rightarrow DB}(298\,K) = 850\,s^{-1}\,. \tag{8}$$

The rate constants of the backward reaction are then given by a combination of Eqs. (7) and (8):

$$k_{21} = k^{HH}_{21} = 2\,k^{HH}_{DB\rightarrow AC} = 10^{12.1\pm0.5}\exp(-47.3 \pm 2.8\ \mathrm{kJ\,mol^{-1}}/RT)\,,\quad 262 \le T \le 310\,K\,,\ 2\,k^{HH}_{DB\rightarrow AC}(298\,K) = 6440\,s^{-1}\,. \tag{9}$$

Table 1
Results of the dynamic ^{1}H- und ^{13}C-NMR-experiments performed on TPP in liquid solution

T/K W_0/Hz	Solvent	Method	k^{HH}/s^{-1}	k^{HD}/s^{-1}	k^{DD}/s^{-1}	D	$\Delta\nu$/Hz	W_0/Hz
198	THF	MTRF	2.3	–	–	0	–	
203	THF	MTRF	2.9	–	–	0	–	
229	Tol	NH	60	–	–	0	99.9	3.3
242	Tol	NH	126	–	–	0	98.2	3.3
249	Tol	NH	196	–	–	0	98.1	3.4
255	Tol	NH	304	–	–	0	97.5	3.2
274	Tol	NH	1180	–	–	0	96.5	3.2
302	Tol	NH	5600	–	–	0	97.2	3.1
273	THF	NH	1400	–	–	0	101.0	–
293	THF	NH	7000	–	–	0	101.0	–
250	THF	$T_{1\varrho}$	243	–	–	0	–	–
270	THF	$T_{1\varrho}$	1120	–	–	0	–	–
280	THF	$T_{1\varrho}$	1740	–	–	0	–	–
259	THF	NH	440[1]	28	–	0.6	98.6	3.7
273	THF	NH	1060[1]	78	–	0.6	97.9	3.5
285	THF	NH	2200[1]	200	–	0.6	97.0	3.0
301	THF	NH	5800[1]	500	–	0.6	97.0	3.5
272	Tol	NH	1040[1]	77	–	0.85	97.4	3.0
280	Tol	NH	1800[1]	154	–	0.85	97.9	2.5
285	Tol	NH	2400[1]	200	–	0.85	97.1	2.5
291	Tol	NH	3800[1]	350	–	0.85	97.0	3.5
300	Tol	NH	5800[1]	700	–	0.85	96.8	3.7
309	Tol	NH	10000[1]	1200	–	0.85	96.8	2.9
321	Tol	NH	25000[1]	2400	–	0.85	96.8	2.5
331	Tol	NH	40000[1]	5600	–	0.85	96.9	2.8
342	Tol	NH	65000[1]	11800	–	0.85	96.9	2.8
72	THF	Py	1060[1]	78[2]	45	0.6/0.9	74[3]	2.0
285	THF	Py	2200[1]	200[2]	120	0.6/0.9	72[3]	2.0
301	THF	Py	5800[1]	500[2]	320	0.6/0.9	71[3]	1.9
312	THF	Py	8000[1]	860[2]	720	0.6/0.9	69[3]	1.6
259	THF	^{13}C	600[1]	–	25	0/0.9	95[3]	5.2
273	THF	^{13}C	1100[1]	160[2]	48	0/0.9	95[3]	4.9
301	THF	^{13}C	8500[1]	–	–	0/0.9	95[3]	4.6
326	THF	^{13}C	28000[1]	5500[2]	–	0/0.9	95[3]	7.6
342	THF	^{13}C	45000[1]	11800[2]	7000	0/0.9	95[3]	4.0

Solvent: Tol = toluene-d_8, THF ≙ tetrahydrofuran-d_8; Method: MTRF ≙ magnetization transfer in the rotating frame [10, 11]; $T_{1\varrho}$: longitudinal relaxation time in the rotating frame [10]; NH: ^{1}H NMR line shape analysis of the ^{1}H-^{15}N signals ($\Delta\nu \triangleq {}^1J_{^1H\text{-}^{15}N}$); Py: ^{1}H NMR line shape analysis of the β-pyrrol signals ($\Delta\nu$ ≙ difference of chemical shifts); ^{13}C: ^{13}C NMR line shape analysis of the β-pyrrole carbon atoms ($\Delta\nu$ ≙ difference of chemical shifts); $k^{LL} = 2 \cdot k^{LL}_{AC\to DB}$, LL = HH, HD und DD; D: deuterium fraction determined by ^{1}H NMR lineshape analysis; W_0: linewidth in the absence of exchange, determined by comparison of signals which do not show exchange broadening; 1: extrapolated values calculated according to Eq.(2); 2: extrapolated values calculated according to Eq.(3); 3: determined by ^{13}C-NMR lineshape analysis using k^{HH} values calculated from Eq.(2).

Table 2
Equilibrium constants K_{12} of the tautomerism in triclinic TPP

T/K	δν/ppm	K_{12}
361	68.6	0.227
343	72.4	0.197
329	75.4	0.176
310	80.7	0.149
202	108.2*)	

*) Difference of the intrinsic chemical shifts $\Delta\nu$.

3.2.3. Mixed Tetragonal Crystal System [(TPP-Ni-$^{14}N_4$)$_{0.1}$(TPP-H_2-$^{15}N_4$)$_{0.9}$]

Fig. 8 shows some representative ^{15}N CPMAS NMR spectra of tetragonal [(TPP-Ni-$^{14}N_4$)$_{0.1}$(TPP-H_2-$^{15}N_4$)$_{0.9}$] (tetragonal TPP) as a function of temperature. These spectra show a spectacular change as compared to those of triclinic TPP. We observed at high temperatures only one sharp singlet, indicating that the equilibrium constant of the tautomerism is equal to 1 within the margin of error. The analysis of the spectra is straightforward and was carried out as in the case of triclinic TTP. The kinetic data are assembled in Table 4. The following temperature dependence of the rate constants was obtained:

$$k_{12} \equiv k^{HH} = 2k^{HH}_{AC\to DB} = 10^{11.8\pm0.3}\exp(-45.4 \pm 1.4\ \text{kJ mol}^{-1}/RT), \quad 243 \le T \le 299\ \text{K},\ 2k^{HH}_{AC\to DB} = 6947\ \text{s}^{-1}. \tag{10}$$

Table 3
Rate constants k_{12} of the tautomerism of triclinic TPP

T/K	262	268	271	273	287	295	300	302	310
k_{12}/s^{-1}	55	70	120	162*)	470*)	789*)	1020	1550*)	2250

further simulation parameters: $\Delta\nu$ = 108.2 ppm; W_o = 41 Hz

*) Data from Ref. [10].

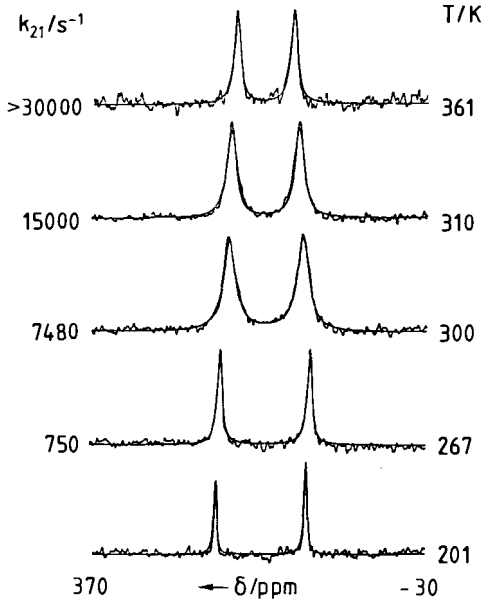

Fig. 7
Superposed experimental and calculated ^{15}N CPMAS NMR spectra of triclinic 5,10,15,20-tetraphenyl-porphyrin (TPP) at 9.12 MHz as a function of temperature. Cross polarization times 15 to 20 ms, 2.7 s repetition time, 7 kHz sweep width, 3 kHz spinning speed. k_{21} is the rate constant of the backward reaction

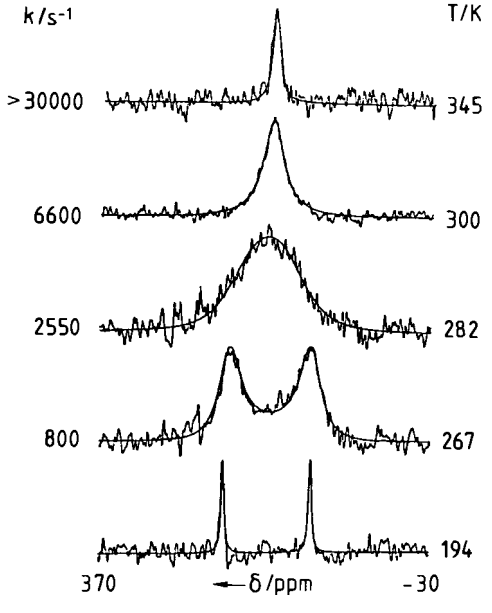

Fig. 8
Superposed experimental and calculated ^{15}N CPMAS NMR spectra of tetragonal [(TPP-Ni-$^{14}N_4$)$_{0.1}$(TPP-H_2-$^{15}N_4$)$_{0.9}$], TPP ≡ 5,10,15,20-tetraphenylporphyrin at 9.12 MHz as a function of temperature. Cross polarization times 15 to 20 ms, 2.7 s repetition time, 7 kHz sweep width, 15000 scans on average, spinning speed >3 kHz

Table 4
Rate constants of the tautomerism of TPP in tetragonal TPP

T/K	243	251	259	267	273	276	282	299
k/s^{-1}	120	180	412	800	1430	1600	2550	6600

further simulation parameters: $\Delta\nu$ = 106.3 ppm; W_0 = 41 Hz

3.3. Results of the NIR Experiments

In Fig. 9 the results of NIR/IR experiments performed on polycrystalline triclinic TPP in the region between 7000 and 6200 cm^{-1} are shown. There are several bands at 6474, 6437, and 6343 cm^{-1} which disappear upon deuteration as also in Fig. 9. This frequency range corresponds to the overtone region of the fundamental NH stretching vibrations. More specifically, the observed bands should correspond to a combination of the asymmetric NH-stretching vibration of TPP appearing at 3318 cm^{-1} and of the symmetric NH-stretching vibration of TPP, whose calculated frequency is 3352 cm^{-1} [13]. The average of both frequencies is then 3335 cm^{-1}. Using the Birge-Sponer equation $\nu_v = v(A + vB)$ [59], where A is the mechanical frequency, B the anharmonicity, $v = 1$ the index of the fundamental and $v = 2$ of the overtone region, we obtained, using ν_1(NH) = 3335 cm^{-1} and ν_2(NH) = 6450 cm^{-1}, the values A = 3445 cm^{-1} and B = −110 cm^{-1}. This anharmonicity is not much larger as found for the CH stretch, which is of the order of 60 cm^{-1} (ν_1(CH) = 3000 cm^{-1}, ν_2(CH) = 6120 cm^{-1}). Similar results were previously observed in the case of the double proton transfer system azophenine [26]. No further attempt was made to study the question of the origin of the band sub-structure.

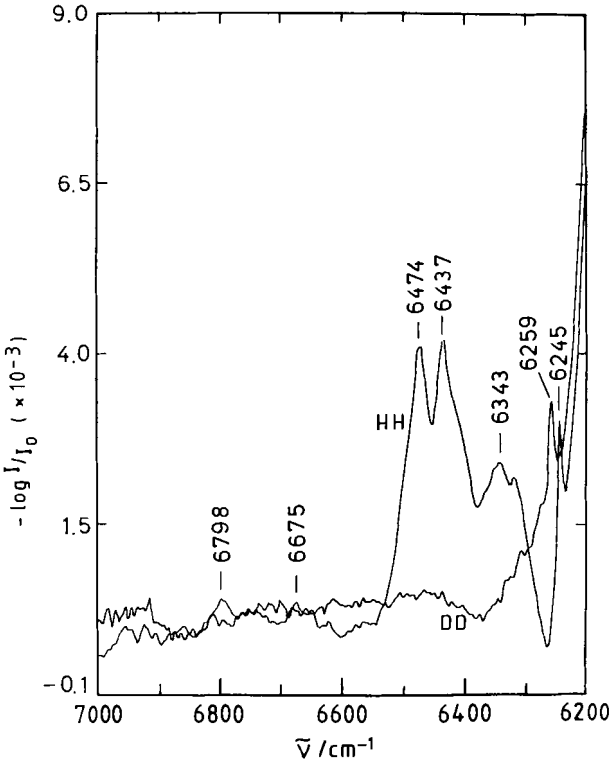

Fig. 9
Experimental NIR spectra of polycrystalline triclinic TPP measured in diffuse reflection on KCl

4. Discussion

We have obtained by NMR improved values of the rate constants of the tautomerism of 5,10,15,20-tetraphenylporphyrin (TPP, Fig. 1) dissolved in organic solvents, including the kinetic HH/HD/DD-isotope effects. In addition, the dynamics of this process were studied for the triclinic and tetragonal polycrystalline TPP phases. In the following, we will first discuss the Arrhenius curves of the isotopic processes. It will be shown that there is evidence for a non-Arrhenius behavior of the rate constants of the hydrogen

migration. The observed kinetic HH/HD/DD isotope and solid state effects are then interpreted. Finally, the information arising from these experiments on the reaction mechanism will be discussed.

4.1. The Arrhenius Curves of the Tautomerism of TPP

In this section, we compare the kinetic data of the tautomerism of TPP obtained for the different phases. In order to facilitate the discussion, the important kinetic data are assembled in Table 5. Firstly, we note that the data obtained for the liquid state tautomerism of TPP found here agree well with the selected data obtained previously. Secondly, we note that the data obtained for TPP dissolved in various solvents and tetragonal TPP can directly be compared since the equilibrium constants of the tautomerism, $K_{AC\rightarrow DB}$ are equal to 1 in both environments. Although there are noticable differences in the activation parameters, the rate constants of the HH process in the different environments coincide within the margin of error which indicates absence of kinetic solid state effects (see Eqs. (2) and (19)). The question then arises as to the origin of the differences in the activation parameters for both phases. A careful analysis shows that this phenomenon arises from the circumstance that the temperature range in which both data sets were obtained are different and that there is a non-Arrhenius behavior of the HH-Arrhenius curve in the sense that the activation energy for the HH motion seems to decrease at lower temperatures. This effect was, in part, observed previously [7]; however, it was overestimated at that time, because the shortening of the transverse relaxation times due to slow molecular tumbling was not considered [8–12]. Note that the rate constants obtained for the HH motion at the lowest temperature stem from magnetization transfer experiments in the rotating frame [10], where slow molecular tumbling does not affect the kinetic results. In order to take the non-Arrhenius behavior into account, the data of the HH tautomerism were fitted to a double exponential. We obtained the following result:

$$k^{HH} = 2k^{HH}_{AC\rightarrow DB} = 10^{12.6}\exp(-51.7\ \text{kJ mol}^{-1}/RT) + 10^{9.6}\exp(-35.5\ \text{kJ mol}^{-1}/RT), \quad 198 < T < 340\ \text{K}. \tag{11}$$

The solid HH-Arrhenius curve in Fig. 10 was calculated according to Eq. (11) and fits the data very well. Its non-linear behavior is well pronounced. However, it must be noted that the solid line in Fig. 10 is not very sensitive to parameter changes in Eq. (11), especially to those of the 2nd term. Thus, Eq. (11) is only valid in the temperature range covered and might be subject to changes if the temperature range is increased. The observed deviation from a linear Arrhenius-relationship is, therefore, probably the beginning of a much larger non-linearity, at even lower temperatures [19, 20]. The curvature gives a good explanation as to why the activation parameters of the TPP tautomerism depend on the temperature range where rate constants are measured. As will be discussed below, this non-linearity is an indication of hydrogen tunneling during the migration process [7, 11, 16–20].

Table 5
Activation parameters of the tautomerism of 5,10,15,20-tetraarylporphyrins

		E_a/ kJ mol^{-1}	log A	$2k_{DB\rightarrow AC}$/ s^{-1}	T-range/K
TPP-H_2	liq	39.6 39.8[1]	10.7 10.9[1]	5600 8450[1]	198–340
TPP-HD	liq	53.1	12.1	580	259–342
TPP-D_2	liq	55.1 56.4[1]	12.2 12.8[1]	326 823[1]	259–342
TPP-H_2	tgn	45.4	11.8	6947	243–299
TPP-H_2	tkl	47.3	12.1	6438	262–310
TTP-H_2	mon	41.9	11.1	5693	204–299

[1] Ref. [11]; (liq ≙ liquid; tkl ≙ triclinic; tgn ≙ tetragonal; mon ≙ monoclinic).

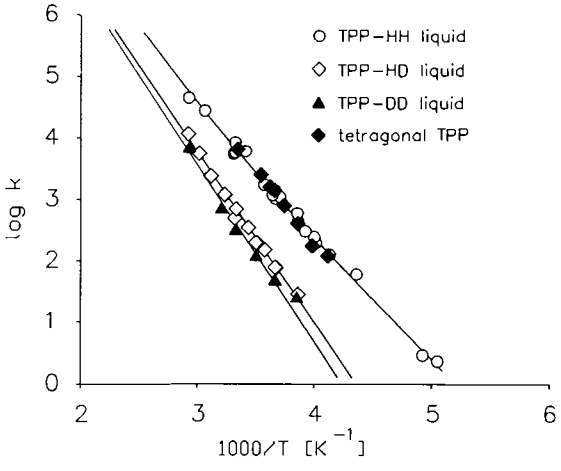

Fig. 10
Arrheniusdiagram of the tautomerism of 5,10,15,20-tetraphenylporphyrin (TPP, Fig. 1). The rate constants k correspond to the quantities $2k^{LL}_{AC\rightarrow DB}$, LL = HH, HD and DD

The solid state experiments on triclinic TPP show that it is possible to manipulate the rate and equilibrium constants of tautomerism of TPP by placing the molecule in different environments, i.e. by changing the intermolecular interactions which in turn change the molecular structure. Fig. 11 shows the Arrhenius curves of the forward and backward reaction rate constants $2k^{HH}_{AC\rightarrow DB}$ and $2k^{HH}_{DB\rightarrow AC}$ of the tautomerism of triclinic TPP. The forward rate constant of triclinic TPP at 298 K is about 6 times smaller as compared to tetragonal TPP, whereas the backward rate constants are of the same order as in tetragonal TPP. The latter observation is demonstrated by the upper solid line in Fig. 11 which represents Eq. (11), i.e. the symmetric rate constants $2k^{HH}_{AC\rightarrow DB} = 2k^{HH}_{DB\rightarrow AC}$ of tetragonal TPP and of TPP dissolved in organic liquids. The lower solid curve was calculated from Eq. (11) using the relation $k^{HH}_{DB\rightarrow AC} = 2^{HH}_{AC\rightarrow DB}/K_{AC\rightarrow DB}$, where $K_{AC\rightarrow DB}$ is the equilibrium constant of the non-degenerate tautomerism. These results are rather sur-

prising, because in terms of the usual Marcus theory [65], one would have predicted an increase of the backward and a decrease of the forward rate constants when the degeneracy is lost. This result will further be discussed below.

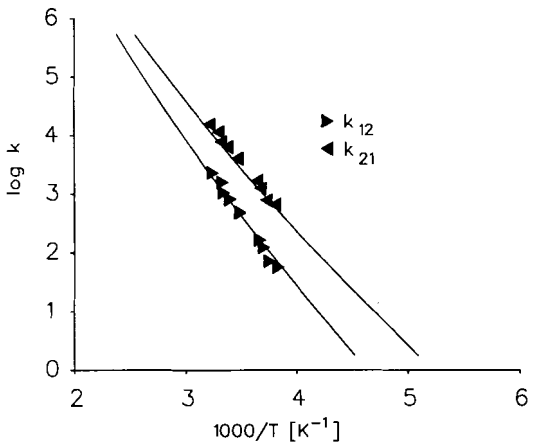

Fig. 11
Arrhenius diagram of the tautomerism of triclinic in the solid state. The data stem from the backward rate constants. The solid line stems from the kinetics of TPP in liquid solution

4.2. The Interpretation of the Kinetic HH/HD/DD Isotope Effects

The first question to be discussed is why the first kinetic isotope effect $k^{HH}/k^{HD} \cong 9.4$ is so much larger than the second kinetic isotope effect $k^{HD}/k^{DD} \cong 1.8$. In our first paper on the determination of kinetic HH/HD/DD isotope effects of degenerate double proton transfer which appeared in 1982 [11], the phenomenon that

$$k^{HH}/k_{HD} \gg 1\,,\quad k^{HD}/k^{DD} \cong 1 \text{ to } 2 \tag{12}$$

was explained with a reaction pathway which involves a concerted tunneling of both protons. Since then, our knowledge of kinetic HH/HD/DD isotope effects in degenerate intra- and intermolecular double proton transfer reactions has evolved, as stated in the introduction. It has now been confirmed that in cases where both protons are "in flight" in the rate limiting step of a double proton transfer, that both k^{HH}/k^{HD} and k^{HD}/k^{DD} are $\gg 1$ [23, 24]. Tunneling may lead to some deviations from the rule of the geometric mean which states that [11, 60]

$$k^{HH}/k^{HD} = k^{HD}/k^{DD}\,. \tag{13}$$

However, experience shows that Eq. (12) is valid in degenerate double proton transfer reactions which involve two consecutive single proton transfer steps via an intermediate. In the case of the oxalamidine tautomerism, this interpretation of a stepwise proton motion was further confirmed by observing a strong kinetic solvent effect which gave evidence of a high intermediate expected for the stepwise reaction mechanism [27].

Theoretical expressions for the kinetic HH/HD/DD isotope effects of the stepwise degenerate proton transfer mechanism of the type AC→AB, DC→DB shown in Fig. 2, where AC and DB, as well as AB and DC are degenerate, have been proposed in Refs. [21b] and [25]. These expressions are based only on formal kinetics, i.e. they are valid both for proton jumps over the barrier as well as for proton tunneling through the barrier:

$$k^{HH}_{AC\to DB} = k^{HH}_{AC\to DC}\,. \tag{14}$$

$$k^{HD}_{AC\to DB} = \frac{2}{S^{-1}+P^{-1}}\,k^{DD}_{AC\to DC} = \frac{2}{P+S}\,k^{HH}_{AC\to DC}\,. \tag{15}$$

$$k^{DD}_{AC\to DB} = k^{DD}_{AC\to DC} = (SP)^{-1}\,k^{HH}_{AC\to DC} = (SP)^{-1}\,k^{HH}_{AC\to DB}\,. \tag{16}$$

P and S are the primary and the secondary kinetic isotope effects of the initial single proton transfer, defined by

$$P = \frac{k^{HL}_{AC\to DC}}{k^{DL}_{AC\to DC}}\,,\quad S = \frac{k^{LH}_{AC\to DC}}{k^{LD}_{AC\to DC}}\,,\quad L = H, D\,. \tag{17}$$

By combination of Eqs. (15) to (17) it follows that

$$S = (k^{HH}_{AC\to DB}/k^{HD}_{AC\to DB}) \cdot [1-\sqrt{1-(k^{HD}_{AC\to DB}/k^{HH}_{AC\to DB})(k^{HD}_{AC\to DB}/k^{DD}_{AC\to DB})}]\,. \tag{18}$$

and that

$$P = (k^{HD}_{AC\to DB}/k^{DD}_{AC\to DB}) \cdot [1-\sqrt{1-(k^{HD}_{AC\to DB}/k^{HH}_{AC\to DB})(k^{HD}_{AC\to DB}/k^{DD}_{AC\to DB})}]^{-1}\,. \tag{19}$$

For the case where S is of the order of 1, one can write in good approximation

$$k^{HD}_{AC\to DB} = \cong 2k^{DD}_{AC\to DB}/(S^{-1} + k^{DD}_{AC\to DB}/k^{HH}_{AC\to DB}) \tag{20}$$

from which it follows that

$$S^{-1} = 2k^{DD}_{AC\to DB}/k^{HD}_{AC\to DB} - k^{DD}_{AC\to DB}/k^{HH}_{AC\to DB}\,. \tag{21}$$

If S were exactly 1, the rate constant $k^{HD}_{AC\to DB}$ would be double the rate constant $k^{DD}_{AC\to DB}$. These results can be visualized in a free energy diagram shown in Fig. 12. In all isotopic reactions there are two equivalent pathways involving either the intermediates AB or DC. The initial and final states AC and DB, as well as the two intermediates AB and DC, have two bound protons leading to three isotopic states of different energy, containing either mobile HH, HD or DD isotopes. By contrast, the states where one proton is in flight are characterized by only two isotopic states of different energy, because there is only one bound hydrogen isotope. Note that the term "state with a proton in flight" can either be a conventional transition state, or a state where the proton tunnels from an activated state through the reaction energy barrier. Let us first compare the HH and the DD reaction profile in Fig. 12. Both profiles are symmetric; therefore, once an intermediate is formed, there is only a probability of 1/2 that the final product D is formed. In terms of transition state theory, there are two true equivalent

transition states. The DD reaction is slower than the HH reaction because approximatively one zero point energy difference is lost in the transition states. By contrast, the reaction profile of the HD process is asymmetric. The two transition states are now of unequal energy. The energy necessary to reach the H-transition states is almost the same as in the HH process and the energy necessary to reach the D-transition states the same as in the DD case, neglecting secondary kinetic isotope effects. The D-transfer step, thus, constitues the rate limiting step of the reaction. Therefore, the HD reaction has the same free energy of activation as the DD reaction; however, since all molecules which have passed the D-transition state react to products by contrast to the DD reaction, it follows that

$$k^{HD}_{AC\rightarrow DB} \cong 2k^{DD}_{AC\rightarrow DB}. \qquad (22)$$

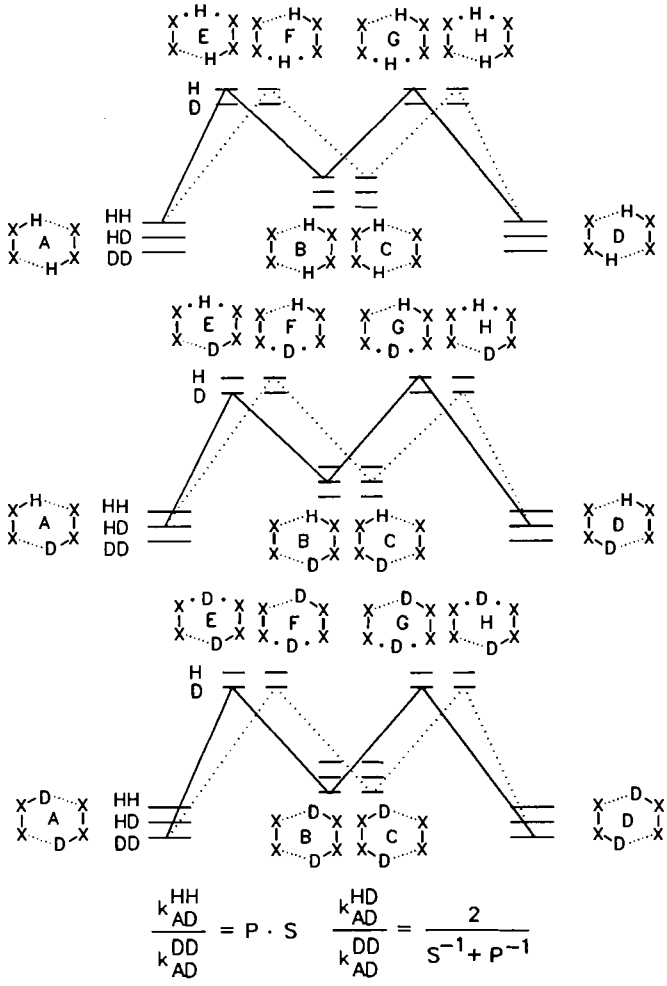

Fig. 12
Free energy diagram of the stepwise reaction pathway of the degenerate HH, HD and the DD tautomerism of porphyrins

Note that Eqs. (19) to (21) were found to accomodate the kinetic data of the degenerate double proton transfers in azophenine [25] and oxalamidine [27]. In the latter case, this interpretation of a stepwise proton could be furthermore corroborated by the discovery of strong kinetic solvent effects due to the formation of highly polar intermediates B and C [27].

Can the experimental kinetic isotope effects of the TPP migration be explained by this theory? From the experimental isotopic rate constants (Eqs. (2) to (4)) we obtained $S = 0.94$ and $P \cong 18$ at 298 K using Eqs. (18) and (19). Similar results are obtained at other temperatures. These values of S are very close to unity as expected for secondary H/D kinetic isotope effects. Thus, Eq. (22) is well fulfilled within the margin of error. The interpretation of the kinetic HH/HD/DD isotope effects of the TPP-tautomerism in the liquid state support a stepwise proton transfer according to Fig. 2. Note that Eq. (20) was already proposed in Ref. [11] for the case where $S = 1$. However, the experimental rate constants $k^{HD}_{AC\rightarrow DB}$ and $k^{DD}_{AC\rightarrow DB}$ were not precise enough in order to detect a difference between the two constants and the stepwise reaction pathway mechanism of the porphyrin tautomerism was not recognized at that time.

4.3. The Role of Tunneling in the Tautomerism of TPP

Since $S \cong 1$, the total kinetic isotope effect $k^{HH}_{AC\rightarrow DB}/k^{DD}_{AC\rightarrow DB}$ is approximately equal to the single primary isotope effect P defined in Eq. (17) of the initial single proton transfer step. The value of $P \cong 18$ at 298 K is larger than observed for the related tautomerism of oxalamidine [27] and of azophenine [25] where values of the order of 3 to 5 were observed at 298 K. Using arguments which were proposed by Bell [61, 62], a large size of P is consistent with a thermally activated tunnel mechanism. In this case, the Arrhenius curve should also show a concave curvature when measured over a wide temperature range. Note that in recent optical studies it was possible to obtain estimates of the rate constants of the thermal tautomerism of the parent compound porphyrin embedded in solid hexane, at temperatures around 100 K [19, 20]. In this temperature region, the rate constants are of the order of hours but the energy of activation was only of the order of 27 kJ mol^{-1}, i.e. less found here. As compared to the kinetic data obtained for TPP in the range between 200 and 300 K, this result represents a strong non-linearity of the Arrhenius curve at lower temperatures. As shown by Eq. (11), a similar non-linearity is also manifest for TPP already at temperatures around 200 K. A direct comparison of the kinetic data of porphyrin and TPP is, however, not possible since the rate constants of TPP are slightly smaller than in porphyrin [41, 66]. Nevertheless, the reaction pathway of the porphyrin reaction evolving from these results, as well as from the theoretical studies [17, 18], can be represented by Fig. 12. Only the symmetric reaction profiles of the HH and the DD reaction are shown. The stable states AC and DB interconvert either via the metastable intermediate AB or DC. At high temperatures, the reaction proceeds over the barrier. The difference of the energies of activation of the HH and the DD reaction is approximately the usual zero point energy difference of a single proton transfer reaction. An estimate of this difference can be obtained by comparing the first term in Eq. (2) with Eq. (4) from which we obtain a value of 6 kJ

mol^{-1}. This corresponds to the loss of the zero point energy of the NH stretching vibration, but possibly also of the bending vibration in the transition state. From this result, one can estimate a value of 6 for the primary kinetic isotope effect P at 298 K. The corresponding experimental value is, however, much larger and is associated with the phenomenon of hydrogen tunneling at lower temperatures from excited vibrational states. If the reaction coordinate were identical to the normal mode of the NH-stretching vibration, as proposed previously [10, 11, 13], only the ground and the first excited NH-stretching state lie below the top of the barrier leading to a greater anharmonicity of the NH-stretching overtones, in contrast to the experimental findings. Thus, the reaction coordinate must also involve bending modes and skeleton vibrational modes as was previously proposed on theoretical grounds [16]. Note, however, that irradiation of the NH-stretching overtones seems to lead to an interconversion of tautomers [20]. As a result, one can claim that there are probably a large number of vibrational states on both sides of the barrier from which tunneling may occur at low temperatures and not just a few NH-stretching states. In the low temperature limit, minimum activation energy is still necessary for tunneling to occur. This free energy corresponds to the energy of the metastable intermediates and is similar to both the protonated and the deuterated system. Therefore, the kinetic HH/DD isotope effects become insensitive to temperature at low temperatures.

4.4. Solid State Effects on the Tautomerism of Tetraarylporphyrins

Let us now discuss what information can be obtained from a comparison of the proton transfer kinetics in the various states of TPP. Firstly, we note that the crystal symmetry of tetragonal TPP enforces that the equilibrium constant of tautomerism, $K_{AC \rightarrow DB}$, is, as expected, close to 1 in this environment. In other words, the different tautomers AC, CA, BD and DB of tetragonal TPP are degenerate, because the molecule experiences a $\bar{4}$ symmetry. The reaction profile is shown schematically in Fig. 13 on the left-hand side. For TPP in liquid solution, the tautomerism is also degenerate within the NMR time scale, but this degeneracy is the consequence of fast molecular motions. In a timescale of slow motion, the degeneracy might be lost as was found for related tetraazaannulenes dissolved in glassy polystyrene [45, 47]. Nevertheless, since the rate constants of tautomerism of tetragonal TPP and of TPP in liquid solution (and also of meso-tetratolylporphyrin [40, 46]) coincide within the margin of error of our NMR experiments, such asymmetries induced in TPP by the solvent molecules seem to be quite small.

The reaction profile for triclinic TPP is shown in Fig. 13 on the right-hand side. As expressed by Eqs. (7) to (9), the tautomers AC ($\equiv$CA) and DB ($\equiv$BD) of TPP in Fig. 2 are not equivalent in the triclinic phase, although the isolated structures are equivalent. There is an energy difference ΔE of the order of 7.5 kJ mol^{-1} betweeen the two forms as expressed in Fig. 13 on the right side which leads to a different population of both tautomers of 9:1 at room temperature. It is understandable that the non-dominant tautomer was not observed by X-ray crystallography [32] due to its small population. As noted above, the kinetic experiments indicate that the energy of activation of the backward reaction is similar to that in the tetragonal form, i.e. it seems that only the energy of the tautomer AC is changed by ΔE as indicated in Fig. 13. It is tempting to explain this observation with the different geometry of TPP in the triclinic and the tetragonal phase. According to the crystal structure, the protonated pyrrole rings A, C and the non-protonated rings B and D in the tautomer AC are not equivalent in the case of triclinic TPP. Furthermore, there is a small angle of 6.6° between the protonated pyrrole units A, C and the porphyrin skeleton. By contrast, the non-protonated pyrrole rings B, D are located close to the molecular plane [32]. This deviation from the molecular plane is absent in the parent compound porphyrin and was therefore attributed to intermolecular contacts between the NH atoms and the phenyl rings [32]. One could then speculate that the van der Waals interaction between the two inner protons is smaller in tautomer AC of triclinic TPP as compared to the BD tautomer leading to the observed decrease of the energy of AC. However, one cannot exclude that the intramolecular distortion of the molecule is responsible only to a minor extent for the different thermodynamic and kinetic behavior of triclinic and of tetragonal TPP. These effects would then

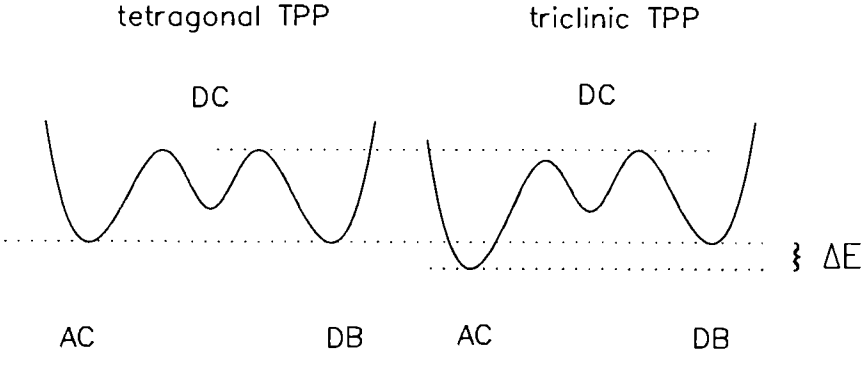

Fig. 13
Left: Reaction profile of the tautomerism of tetragonal TPP; Right: Reaction profile of the tautomerism of triclinic TPP

arise directly from intermolecular interactions. Anyway, the kinetic data indicate similar molecular geometries of TPP in the tetragonal phase and in the liquid solution.

5. Conclusions

In view of recent progress made in the NMR-instrumentation and the understanding of the kinetic HH/HD/DD isotope effects on degenerate double proton transfer reactions, we have re-investigated these effects for the tautomerism of 5,10,15,10-tetraphenylporphyrin (TPP, Fig. 1). Thus, experimental evidence has been obtained for a stepwise reaction mechanism with contributions of incoherent hydrogen tunneling at low temperatures. Solid state NMR measurements show that the reaction energy potential of TPP can be influenced by placing the molecule in different solid environments. In triclinic TPP, the barrier for proton transfer is raised in comparison to tetragonal TPP and to TPP in liquid solution. Also, the degeneracy of the proton tautomerism in the latter two environments is lost in triclinic TPP. It seems that an interplay of inter- and intramolecular interactions are responsible for these solid state effects.

We are indebted to Dr. G. Zachmann, Bruker Analytische Meßtechnik for measuring the NIR-spectra of triclinic TPP. We thank the Deutsche Forschungsgemeinschaft, Bonn-Bad Godesberg, the Stiftung Volkswagenwerk, Hannover, and the Fonds der Chemischen Industrie for financial support.

References

[1] C. B. Storm and Y. Teklu, J. Am. Chem. Soc. *94*, 53 (1974); C. B. Storm and Y. Teklu, Ann. N. Y. Acad. Sci. *206*, 631 (1973).
[2] R. J. Abraham, G. E. Hawkes, and K. M. Smith, Tetrahedron Lett. 1483 (1974).
[3] H. J. C. Yeh, J. Magn. Reson. *28*, 365 (1977).
[4] S. S. Eaton and G. R. Eaton, J. Am. Chem. Soc. *99*, 1603 (1977).
[5] D. Gust and J. D. Roberts, J. Am. Chem. Soc. *99*, 3637 (1977).
[6] C. S. Irving and A. Lapidot, J. Chem. Soc. Chem. Commun. 184 (1977).
[7] J. Hennig and H. H. Limbach, J. Chem. Soc., Faraday Trans. 2 *75*, 752 (1979).
[8] J. Hennig and H. H. Limbach, J. Am. Chem. Soc. *106*, 292 (1984).
[9] P. Stilbs and M. E. Moseley, J. Chem. Soc. Faraday 2 *76*, 729 (1980); P. Stilbs, J. Magn. Reson. *58*, 152 (1984).
[10] J. Hennig and H. H. Limbach, J. Magn. Reson. *49*, 322 (1982).
[11] H. H. Limbach, J. Hennig, D. Gerritzen, and H. Rumpel, Faraday Discuss. Chem. Soc. *74*, 822 (1982).
[12] H. H. Limbach and J. Hennig, J. Chem. Phys. *71*, 3120 (1979).
[13] H. H. Limbach, J. Hennig, and J. Stulz, J. Chem. Phys. *78*, 5432 (1983).
[14] H. H. Limbach, J. Chem. Phys. *80*, 5343 (1984).
[15] V. A. Kutzmitsky and K. N. Solovyov, J. Mol. Struct. *65*, 219 (1980).
[16] A. Sarai, J. Chem. Phys. *76*, 5554 (1982); ibid. *80*, 5431 (1984).
[17] K. M. Merz and C. H. Reynolds, J. Chem. Soc. Chem. Commun. 90 (1988).
[18] Z. Smedarchina, W. Siebrand, and F. Zerbetto, Chem. Phys. *136*, 285 (1989).
[19] H. H. Limbach, personal communication to T. Butenhoff and C. B. Moore; T. Butenhoff and C. B. Moore, J. Am. Chem. Soc. *110*, 8336 (1988).
[20] T. Butenhoff, R Chuck, H. H. Limbach, and C. B. Moore, J. Phys. Chem. *94*, 7847 (1990).
[21] M. Schlabach, H. Rumpel, and H. H. Limbach, Angew. Chem. *101*, 84 (1989); Angew. Chem. Int. Ed. Engl. *28*, 76 (1989); M. Schlabach, G. Scherer, and H. H. Limbach, J. Am. Chem. Soc. *113*, 3550 (1991).
[22] H. H. Limbach, Dynamic NMR Spectroscopy in the presence of Kinetic Hydrogen/Deuterium Isotope Effects in NMR – Basic Principles and Progress, Vol. 23, Chapter 2, Springer, Heidelberg 1990.
[23] D. Gerritzen and H. H. Limbach, J. Am. Chem. Soc. *106*, 869 (1984).
[24] H. H. Limbach, L. Meschede, and G. Scherer, Z. Naturforsch. *44a*, 459 (1989); L. Meschede and H. H. Limbach, J. Phys. Chem. *95*, 10267 (1991).
[25] H. Rumpel and H. H. Limbach, J. Am. Chem. Soc. *111*, 5429 (1989).
[26] H. Rumpel, H. H. Limbach, and G. Zachmann, J. Phys. Chem. *93*, 1812 (1989).
[27] G. Scherer and H. H. Limbach, J. Am. Chem. Soc. *111*, 5946 (1989); G. Scherer, Dissertation Universität Freiburg 1990.
[28] L. E. Webb and E. B. Fleischer, J. Chem. Phys. *43*, 3100 (1965).
[29] B. M. L. Chen and A. Tulinsky, J. Am. Chem. Soc. *94*, 4144 (1972).
[30] A. Tulinsky, Ann. N. Y. Acad. Sci. *206*, 47 (1973).
[31] M. J. Hamor, T. A. Hamor, and J. L. Hoard, J. Am. Chem. Soc. *86*, 1338 (1964).
[32] S. J. Silvers and A. Tulinsky, J. Am. Chem. Soc. *89*, 3331 (1967).
[33] R. J. Butcher, G. B. Jameson, and C. B. Storm, J. Am. Chem. Soc. *107*, 278 (1985).
[34] S. Völker and J. H. van der Waals, Mol. Phys. *32*, 1703 (1976).
[35] S. Völker and R. Macfarlane, IBM Res. Develop. *23*, 547 (1979).
[36] J. Friedrich and D. Haarer, Angew. Chem. *96*, 96 (1984); Angew. Chem .Int. Ed. *23*, 113 (1984).
[37] J. Schaeffer and E. O. Stejskal, J. Am. Chem. Soc. *98*, 1031 (1976).
[38] C. A. Fyfe, Solid State NMR for Chemists, C.F.C. Press, Guelph, Ontario 1983.
[39] J. R. Lyerla, C. S. Yannoni, and C. A. Fyfe, Acc. Chem. Res. *15*, 208 (1982).
[40] H. H. Limbach, J. Hennig, R. D. Kendrick, and C. S. Yannoni, J. Am. Chem. Soc. *106*, 4059 (1984).
[41] B. Wehrle, H. H. Limbach, M. Köcher, O. Ermer, and E. Vogel, Angew. Chem. *99*, 914 (1987); Angew. Chem. Int. Ed. Engl. *26*, 934 (1987).
[42] R. D. Kendrick, S. Friedrich, B. Wehrle, H. H. Limbach, and C. S. Yannoni, J. Magn. Reson. *65*, 159 (1985).
[43] H. H. Limbach, B. Wehrle, H. Zimmermann, R. D. Kendrick, and C. S. Yannoni, J. Am. Chem. Soc. *109*, 929 (1987).
[44] H. H. Limbach, B. Wehrle, H. Zimmermann, R. D. Kendrick, and C. S. Yannoni, Angew. Chem. *99*, 241 (1987); Angew. Chem. Int. Ed. Engl. *26*, 247 (1987).
[45] B. Wehrle, H. Zimmermann, and H. H. Limbach, Ber. Bunsenges. Phys. Chem. *91*, 941 (1987).
[46] H. H. Limbach, B. Wehrle, M. Schlabach, R. Kendrick, and C. S. Yannoni, J. Magn. Reson. *77*, 84 (1988).
[47] B. Wehrle, H. H. Limbach, and H. Zimmermann, J. Am. Chem. Soc. *110*, 7014 (1988).
[48] L. Frydman, A. C. Olivieri, L. E. Diaz, B. Frydman, F. G. Morin, C. L. Mayne, D. M. Grant, and A. D. Adler, J. Am. Chem. Soc. *110*, 8336 (1988).
[49] L. Frydman, A. C. Olivieri, L. E. Diaz, B. Frydman, I. Kustanovich, and S. Vega, J. Am. Chem. Soc. *111*, 7001 (1989).
[50] L. Frydman, A. C. Olivieri, L. E. Diaz, A. Valasinas, and B. Frydman, J. Am. Chem. Soc. *110*, 5651 (1988).
[51] B. Wehrle and H. H. Limbach, Chem. Phys. *136*, 223 (1989).
[52] G. Donnay and C. B. Storm, Mol. Cryst. *2*, 287 (1967).
[53] M. L. Schneider, J. Chem. Soc. 1093 (1972).
[54] A. D. Adler and F. R. Longo, J. Org. Chem. *32*, 476 (1967).
[55] F. R. Longo, E. J. Thorne, A. D. Adler, and S. Dym, J. Heterocycl. Chem. *12*, 1305 (1975).
[56] G. H. Barnett, M. F. Hudson, and K. M. Smith, Tetrahedron 2887 (1973).

[57] A. D. Adler and F. R. Longo, J. Inorg. Nucl. Chem. *32*, 2443 (1970).
[58] E. B. Fleischer, C. K. Miller, and L. E. Webb, J. Am. Chem. Soc. *86*, 2342 (1964).
[59] R. T. Birge and H. Sponer, Phys. Rev. *28*, 259 (1926).
[60] R. D. Gandour and R. L. Schowen, Transition States of Biochemical Processes, Plenum Press, New York 1978.
[61] R. P. Bell, The Tunnel Effect in Chemistry, Chapman and Hall, London 1980.
[62] L. Melander and W. H. Saunders, Reaction Rates of Isotopic Molecules, John Wiley & Sons, New York, Toronto 1980.
[63] P. W. Codding and A. Tulinsky, J. Am. Chem. Soc. *94*, 4151 (1972).
[64] J. W. Lauher and J. A. Ibers, J. Am. Chem. Soc., *95*, 5148 (1973).
[65] R. H. Marcus, J. Phys. Chem. *72*, 891 (1968).
[66] M. Schlabach, Dissertation Universität Freiburg 1989.

(Received: February 20th, 1991) E 7917